

Gemini/GMOS imaging of globular clusters in the Virgo galaxy NGC 4649 (M60)

Duncan A. Forbes,^{1★} Favio Raul Faifer,^{2★} Juan Carlos Forte,^{2★} Terry Bridges,^{3★} Michael A. Beasley,^{1,4★} Karl Gebhardt,^{5★} David A. Hanes,^{3★} Ray Sharples^{6★} and Stephen E. Zepf^{7★}

¹Centre for Astrophysics & Supercomputing, Swinburne University, Hawthorn, VIC 3122, Australia

²CONICET and Facultad de Cs. Astronomicas y Geofisicas, UNLP, Paseo del Bosque 1900, La Plata, Argentina

³Department of Physics, Queen's University, Kingston, ON K7L 3N6, Canada

⁴Lick Observatory, University of California, Santa Cruz, CA 95064, USA

⁵Astronomy Department, University of Texas, Austin, TX 78712, USA

⁶Department of Physics, University of Durham, South Road, Durham DH1 3LE

⁷Department of Physics and Astronomy, Michigan State University, East Lansing, MI 48824, USA

Accepted 2004 August 20. Received 2004 August 20; in original form 2004 May 31

ABSTRACT

We present Sloan g and i imaging from the Gemini Multi-object Spectrograph (GMOS) instrument on the Gemini North telescope for the globular cluster (GC) system around the Virgo galaxy NGC 4649 (M60). Our three pointings, taken in good seeing conditions, cover an area of about 90 square arcmin. We detect 2151 unresolved sources. Applying colour and magnitude selection criteria to this source list gives 995 candidate GCs. Our source list is greater than 90 per cent complete to a magnitude of $i = 23.6$, and has little contamination from background galaxies. We find fewer than half a dozen potential ultracompact dwarf galaxies around NGC 4649. Foreground extinction from the nearby spiral NGC 4647 is limited to be $A_V < 0.1$. We confirm the bimodality in the GC colour distribution found by earlier work using *Hubble Space Telescope*/WFPC2 imaging. As is commonly seen in other galaxies, the red GCs are concentrated towards the centre of the galaxy, having a steeper number density profile than the blue GC subpopulation. The varying ratio of red-to-blue GCs with radius can largely explain the overall GC system colour gradient. The underlying galaxy starlight has a similar density profile slope and colour to the red GCs. This suggests a direct connection between the galaxy field stars and the red GC subpopulation. We estimate a total GC population of 3700 ± 900 , with the uncertainty dominated by the extrapolation to larger radii than observed. This total number corresponds to a specific frequency $S_N = 4.1 \pm 1.0$. Future work will present properties derived from GMOS spectra of the NGC 4649 GCs.

Key words: globular clusters: general – galaxies: individual: NGC 4649 – galaxies: star clusters.

1 INTRODUCTION

The study of globular cluster (GC) systems provides important insights into the star formation history and chemical enrichment of galaxies (Ashman & Zepf 1998; Harris 2001). GCs are created during the initial stages of galaxy formation; but they also appear to

form in subsequent star formation episodes up to, and including, the current epoch. Observationally, GC systems typically reveal a bimodal colour distribution, indicating discrete GC sub-populations (e.g. Gebhardt & Kissler-Patig 1999; Larsen et al. 2001; Kundu & Whitmore 2001)

Several testable galaxy formation scenarios address the origin of this bimodal behaviour (Ashman & Zepf 1992; Forbes, Brodie & Grillmair 1997; Cote, Marzke & West 1998). Recently, GC formation has been placed in the broader cosmological context of galaxy formation. For example, Beasley et al. (2002) investigated the formation of GCs in a semi-analytic model which invoked hierarchical merging in a cold dark matter (CDM) cosmology, finding that blue

*E-mail: dforbes@astro.swin.edu.au (DAF); favio@fcaglp.fcaglp.unlp.edu.ar (FRF); forte@fcaglp.fcaglp.unlp.edu.ar (JCF); tjb@astro.queensu.ca (TB); mbeasley@ucolick.org (MB); gebhardt@astro.as.utexas.edu (KG); hanes@astro.queensu.ca (DAH); R.M.Sharples@dur.ac.uk (RMS); zepf@pa.msu.edu (SEZ)

(metal-poor) GCs are formed at high redshift in protogalactic fragments, while the red (metal-rich) GCs are formed later, during the gas-rich merging of these fragments. One prediction of this model is that the formation of the red GCs will be extended over several Gyr in low-density environments.

In order to test the model predictions, and further probe the halos of galaxies, we have undertaken to study the GC systems in a sample of early-type galaxies with the Gemini telescopes. The galaxies cover a range of environments and luminosities. Our basic approach, using the Gemini Multi-object Spectrograph (GMOS) instruments, is to obtain deep imaging of several fields around each galaxy. A subset of the brighter candidate GCs are then selected for follow-up multi-object spectroscopy (these will be presented in a future paper by Bridges et al., in preparation). The spectra allow us to derive GC system kinematics plus age and metallicity estimates for individual GCs. Some initial results of our programme have been highlighted in Bridges et al. (2003).

In this paper, we present and discuss the results from our deep imaging of the GC system around NGC 4649 (M60). This giant Virgo elliptical lies in a subclump to the east of the main Virgo concentration. The galaxy has strong X-ray emission with a luminosity of $L_X = 2.1 \times 10^{41} \text{ erg s}^{-1}$ (O'Sullivan, Forbes & Ponman 2001), largely from a hot diffuse halo. *Chandra* imaging reveals the presence of numerous discrete sources which are identified as low mass X-ray binaries (LMXBs), some of which lie in GCs (Sarazin et al. 2003). The galaxy has an old stellar population with no evidence of a young central population (Terlevich & Forbes 2002).

The GC system of NGC 4649 was first studied by Couture, Harris & Harris (1991). Their *B* and *V* CCD imaging covered an area of 2.1×3.4 arcmin, and reached a depth of $B \sim 24.5$. They measured a mean colour of $B - V = 0.75$ for 82 candidate GCs but could not detect any bimodality in the colour distribution. A radial colour gradient was seen in the overall GC population. Harris et al. (1991) studied the *B*-band GC luminosity function. These data reached a depth of $B \sim 26$. They measured the turnover to be $B = 24.47 \pm 0.18$ with a Gaussian spread of $\sigma = 1.29 \pm 0.12$. They also showed that the overall GC system has a more extended radial distribution than the underlying starlight.

Larsen et al. (2001) included NGC 4649 in their *HST*/WFPC2 study of GC systems in 17 galaxies, and detected a bimodal GC colour distribution. To $V = 25$, they detected 176 blue GCs and 169 red GCs with mean colours of $(V - I)_0 = 0.954$ and $(V - I)_0 = 1.206$. Kundu & Whitmore (2001) also found bimodality with peaks around $V - I = 0.95$ and 1.20. Larsen et al. fit a t_5 profile to the GC luminosity function and found a peak magnitude of $V = 23.58 \pm 0.08$ and $\sigma = 1.28 \pm 0.09$. The red peak was 0.2 mag fainter than the blue peak. The specific frequency in the literature is relatively high, with $S_N = 6.7 \pm 1.4$ (Ashman & Zepf 1998). In this paper we assume a distance to NGC 4649 of $m - M = 31.13$ (Tonry et al. 2001) or 16.83 Mpc, which implies 1 arcsec = 81 pc. The total *V* magnitude from the RC3 is 8.84. The Galactic extinction is $A_V = 0.086$ from Schlegel, Finkbeiner & Davis (1998) and $A_V = 0.030$ from Burstein & Heiles (1982). This gives $V_0 = 8.75$ (8.81) which corresponds to an absolute magnitude of $M_V = -22.38$ (-22.32). At a projected distance of 12 kpc from NGC 4649 lies the SBc spiral NGC 4647.

2 OBSERVATIONS AND INITIAL DATA REDUCTION

Images were taken of NGC 4649 using the GMOS in imaging mode on the Gemini North telescope on 2002 April 10, 11 and 14. The

internal Gemini program ID is 20020410-GN-2002A-Q-21/Q-13. The instrument consists of three 2048×4608 pixel CCDs, with a scale of $0.072 \text{ arcsec pixel}^{-1}$, yielding a $5.5 \times 5.5 \text{ arcmin}^2$ field-of-view in a single pointing. We obtained three pointings close to the galaxy centre: the north-east (field No. 1), south-east (field No. 2), and east (field No. 3). The images were taken using modified Sloan *g* and *i* filters (centred at wavelengths of 475 and 780 nm, respectively). Both *g* and *i* images had exposure times of $4 \times 120 \text{ s}$, and the subexposures were dithered to remove the gaps between the CCD chips. The seeing for the three fields were similar in the *g* and *i* filters, with 0.6, 0.7 and 1.0 arcsec for field Nos 1, 2 and 3, respectively.

The raw images were processed using the Gemini GMOS routines within IRAF (e.g. GPREPARE, GBIAS, GIFLAT, GIREDUCE and GMOSAIC). The resulting images for each filter were then co-added using IMCOADD. These images were then used for all the subsequent data analysis.

3 OBJECT FINDING AND SELECTION

3.1 Galaxy halo removal

To aid in the selection, classification and photometry of the GC candidates we must first remove the bright background of the galaxy halo.

After experimenting with different filtering and modelling methods we adopted the SExtractor (Bertin & Arnouts 1996) background modelling approach. This method makes a local estimate of the background by, first, selecting a number of pixels within a box that, after *k*-sigma clipping and median filtering, yields a mesh of background values. These values can then be interpolated in order to estimate the background level at a given position. The best results were obtained for a grid sampling of 32 by 32 pixels, combined with a 5-pixel (square box) median filter, and bi-cubic interpolation.

3.2 Determination of the point spread function

The determination of the point spread function (psf) on the co-added images was made using the DAOPHOT II package (Stetson 1987) within IRAF. Each psf determination involved 30 to 60 objects per field and the use of the variable psf option. Some of the unresolved objects (i.e. the brightest and relatively uncrowded ones) were used to derive aperture corrections to the psf fitting photometry.

An object search was carried out on the *i* image, as this is the deepest in terms of signal-to-noise ratio, using the finding routines included in the SExtractor package. This approach classifies a detection as real if it is composed of a number of connected pixels, above a certain signal-to-noise ratio. We used the following SExtractor parameters: detection threshold of 1.5 sigma; detection minimum area of 3 pixel, and filtering with a Gaussian of full width at half maximum (FWHM) of 0.58 arcsec.

A size measure (i.e. resolved or unresolved) for each object was made in two steps. The stellarity index, defined in SExtractor, was used as a first step. This index takes values of around 1.0 for unresolved objects and close to 0.0 for extended ones (at the distance of NGC 4649, GCs are not resolved in the GMOS images).

Fig. 1 shows the behaviour of the stellarity index as a function of the *i* magnitude and shows that, for a range of intermediate index values, the nature of a given object cannot be unambiguously identified. However, from a sample of 7000 artificial objects created with the ADDSTARS routine, we found that a stellarity index of greater than

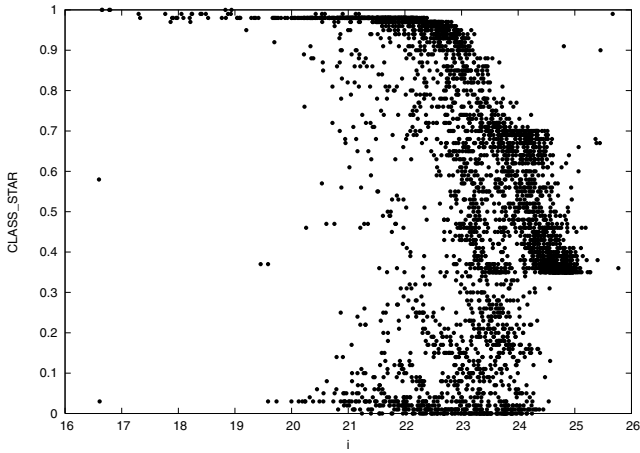


Figure 1. SE extractor stellerity index as a function of i magnitude for all the objects found in the composite mosaic field. Initially, all objects with an index >0.35 were selected as unresolved.

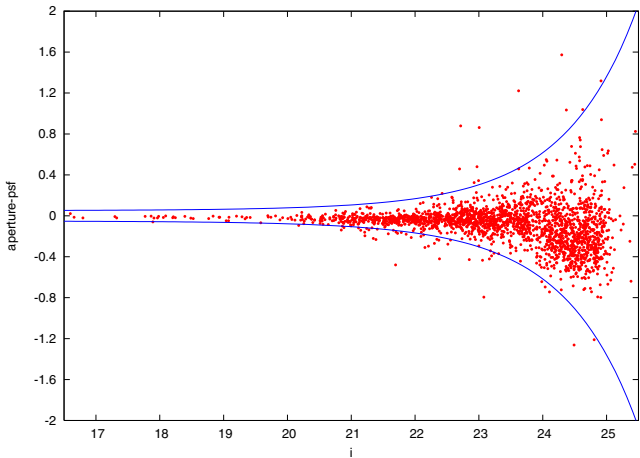


Figure 2. Aperture-minus-psf magnitude versus i psf magnitude for all the objects with stellerity index larger than 0.35. The solid lines define the upper and lower boundaries of the region occupied by objects that were finally classified as unresolved.

0.35 provided a good initial definition of ‘unresolved’ (i.e. less than 1.5 per cent of objects were misclassified).

In order to improve this first selection, we analyzed the position of each object on a psf magnitude versus aperture-minus-psf magnitude diagram shown in Fig. 2. This figure shows both an increase of the dispersion as a function of magnitude, as expected from increasing photometric errors, and also an asymmetry towards negative values that is indicative of the resolved nature of the images. The upper boundary (positive values) in this figure is presumably dominated by unresolved objects and was quantified by adopting an exponential fit. This curve, and its negative mirror, were then used to define the domain of what we consider as unresolved objects. All those objects with magnitude differences more negative than the lower curve were then removed and added to the resolved objects list. Thus, we have a list of 874 resolved objects (i.e. galaxies) and a list of 2151 unresolved objects, i.e. candidate GCs.

Figs 3 and 4 show the spatial distribution of the GC candidates and of the resolved objects. There is a clear concentration of the

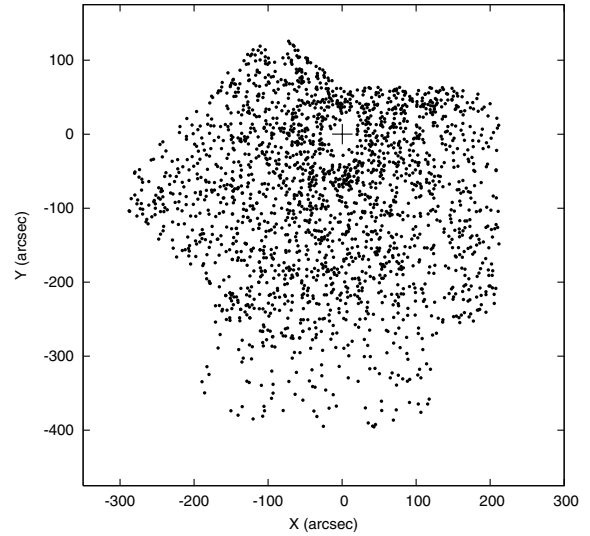


Figure 3. Location of all 2151 unresolved objects around NGC 4649 in arcsec (each pixel is 0.072 arcsec). North is up and east is to the left. There is a clear concentration around the galaxy centre (indicated by a cross).

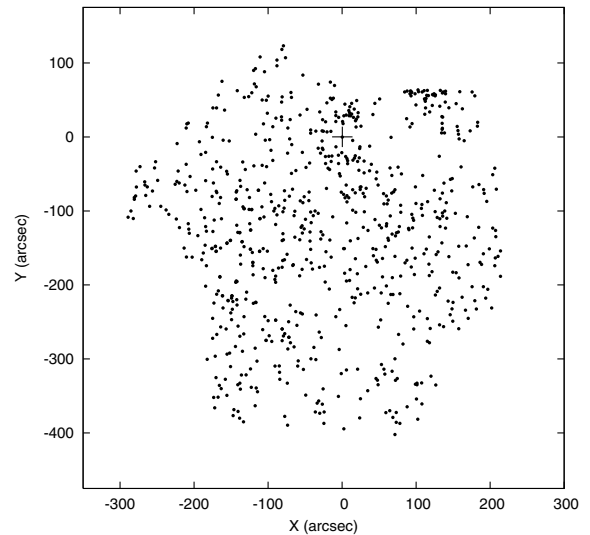


Figure 4. Location of all 874 resolved objects around NGC 4649 in pixels. North is up and east to the left. The spatial distribution appears largely random in nature.

candidate GCs around the galaxy, whereas the resolved objects have a more random spatial distribution.

3.3 Photometry

One of the pointings (field No.1) exhibits the best overall seeing both for the g and i images and was adopted as the reference field, i.e. both the instrumental (psf) magnitudes and colours of the other two pointings were derived using objects in the overlapping regions. After atmospheric extinction correction, the instrumental magnitudes and colours were linked to the standard system by adopting the zero-point values provided by the Gemini pipeline. We expect the absolute photometric calibration of GMOS images to improve with time, so our calibration should be considered as preliminary. The behaviour of the photometric errors for candidate GCs (as derived

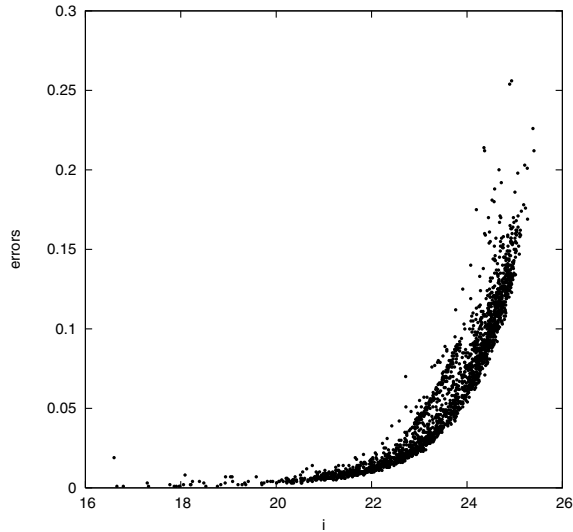


Figure 5. The i magnitude errors as a function of magnitude for the globular cluster candidates listed in Table 1. Typical errors are ± 0.08 mag at $i = 24$.

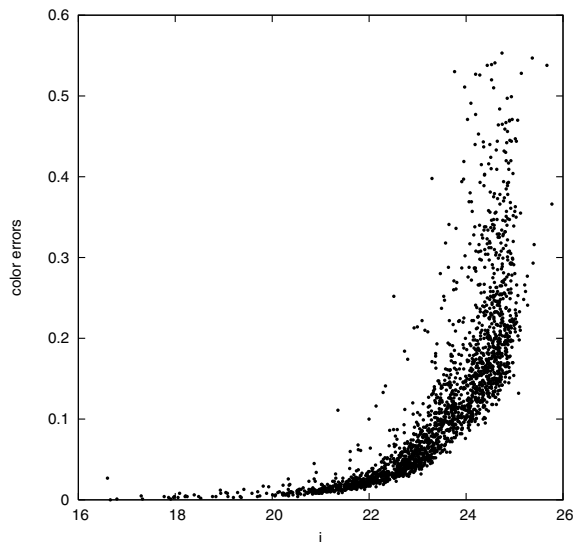


Figure 6. The $(g - i)$ colour errors as a function of the i magnitude for the globular cluster candidates listed in Table 1. Typical colour errors are ± 0.13 mag at $i = 24$.

from the DAOPHOT package) are shown in Figs 5 and 6. Typical errors at $i = 24$ are 0.08 in magnitude and 0.13 in colour.

Note that the magnitudes and colours presented in this paper have *not* been corrected for Galactic extinction. The extinction values from Schlegel et al. (1998, $A_V = 0.086$) and from Burstein & Heiles (1982, $A_V = 0.030$), with $A_g = 1.25A_V$ and $A_i = 0.65A_V$, imply a colour reddening correction of 0.052 and 0.018, respectively. If we apply the g, i to V, I transformations of Smith et al. (2002), our colours are ~ 0.05 mag redder than the Schlegel et al. extinction-corrected values given in Larsen et al. (2001). This suggests that our magnitudes, although preliminary, are close to the standard photometric system.

Table 1 gives the photometry for the candidate GCs (similar measurements for the resolved objects are given in the Appendix Table A1). We list x -, y -position (in pixels), defined in a rectangular

Table 1. Candidate NGC 4649 globular clusters.

X (pix)	Y (pix)	R_{GC} (arcsec)	i (mag)	$g - i$ (mag)	i err (mag)	$g - i$ err (mag)
3479	4546	101.6	22.95	1.11	0.03	0.06
4284	4546	151.3	21.19	0.99	0.01	0.01
4048	4541	135.8	20.51	0.67	0.01	0.01
...

Notes: the full table is available in the on-line version at <http://www.blackwellpublishing.com/products/journals/suppmat/MNR/MNR8333/MNR8333sm.htm>

system with its origin at the galaxy centre with x positive towards west and y positive towards the north; galactocentric radius (in arcsec), i magnitude, $g - i$ colour and their errors.

3.4 Completeness experiments

An estimate of the completeness of the photometric sample given in Table 1 was carried out by means of ADDSTARS experiments conducted on the i band galaxy-subtracted image. A total number of 7000 artificial objects were added to the image and the identification routine was run using the same search parameters as before. The spatial distribution of the artificial objects was determined using a stochastic-generating program that, in an approximate way, follows the radial distribution of the globular cluster candidates.

The results of our completeness tests are shown in Figs 7 and 8. Fig. 7 shows the overall magnitude completeness, indicating that at $i = 23.4$ the data are 90 per cent complete and at $i = 24.7$ the data are 50 per cent complete. However, our completeness varies with galactocentric radius. In Fig. 8 we show the completeness fractions for several different ranges of magnitude as a function of galactocentric radius. This figure shows that for i magnitudes brighter than 23.4, we have detected the vast majority of GCs over the entire NGC 4649 field. For magnitudes fainter than $i = 23.4$, we are missing some of the innermost GCs.

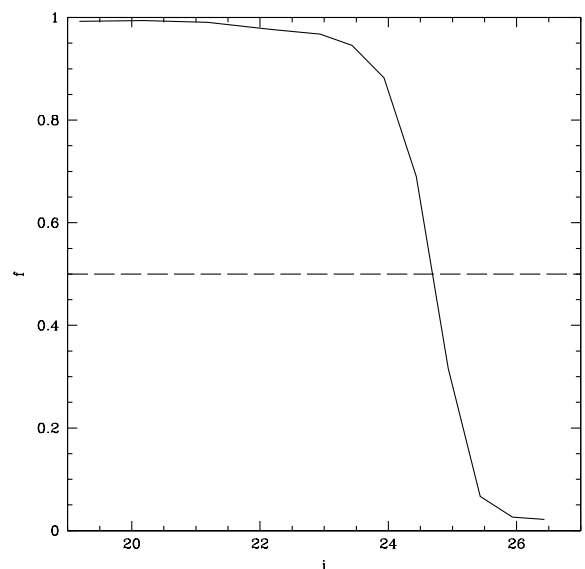


Figure 7. Overall completeness fraction as a function of i magnitude. The horizontal line shows the 50 per cent completeness level corresponding to a magnitude of $i \sim 24.7$.

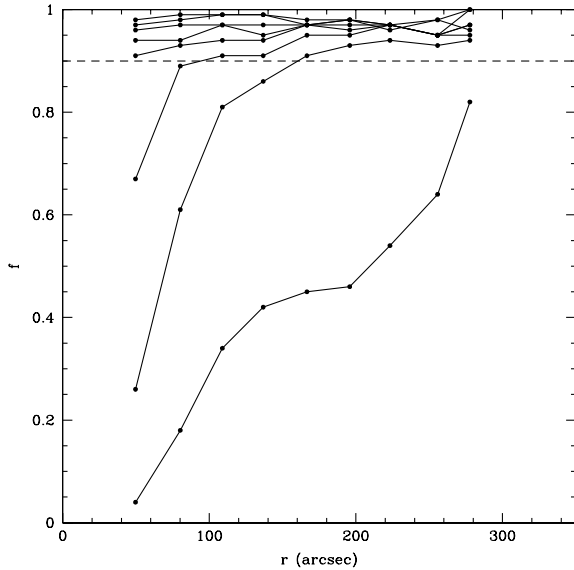


Figure 8. Completeness fraction as a function of galactocentric radius for the entire NGC 4649 field, after galaxy halo subtraction. The curves show the completeness (from top to bottom) for $i = 19.14, 20.14, 21.14, 22.14, 22.9, 23.4, 23.9$ and 24.4 . The horizontal line shows the 90 per cent completeness level.

3.5 Background contamination

The degree of background contamination for the objects listed in Table 1 was estimated by adopting a comparison field, and assuming it is representative of the background near NGC 4649. This field was observed as part of our overall Gemini program, and is located some distance from the galaxy NGC 7332. Objects in the comparison field were selected using a similar procedure to that for the NGC 4649 fields. The number of resolved objects (i.e. presumably background galaxies) in the comparison field was found to be 256. This is consistent with the 874 resolved objects found in the three galaxy fields given the slight seeing variations between fields. We note also, that we find 38 non-resolved objects (i.e. presumably foreground stars) in the comparison field. The galaxy model of Ratnatunga & Bahcall (1985) predicts 22 in our magnitude and colour range.

After completeness tests, similar to those described above, we find that the background field has a similar magnitude completeness to the NGC 4649 data with the 50 per cent completeness fraction occurring at $i \sim 24.7$. From this comparison field, we estimate the contamination of background objects in our sample of candidate GCs to be ~ 3 per cent for $i < 24$. Thus we can be confident that the effects of background objects on the results presented below are minimal.

4 FOREGROUND DUST FROM NGC 4647?

The spiral galaxy NGC 4647 (UGC 7896) is located to the north-west (position angle $PA \sim -45^\circ$) of NGC 4649 at a projected separation of about 12 kpc. It has a recession velocity of 1422 km s^{-1} , or 305 km s^{-1} greater than that of NGC 4649. There are no obvious tidal interaction signatures between the two galaxies. Images of NGC 4647 reveal a flocculent spiral structure with strong dust lanes. If NGC 4647 lies in the foreground then dust in its outer regions may cause reddening of the NGC 4649 GCs in the north-west quadrant.

We have compared both the GCs and the underlying starlight in the north-west quadrant to each of the other three quadrants. We find similar colours ($\Delta g - i < 0.1$) and similar mean magnitudes ($\Delta i < 0.05$). These limit the extinction to be $A_V < 0.1$. In a study of dust extinction in overlapping galaxies, White, Keel & Conselice (2000) concluded that if NGC 4647 caused any additional extinction in NGC 4649 then it was limited to $A_B < 0.11$. Thus with no evidence for strong foreground dust reddening due to NGC 4647, we proceed to treat all GCs the same.

5 RESULTS

5.1 Globular cluster colours

A colour–magnitude diagram for the candidate GCs is shown in Fig. 9. The diagram shows some evidence of colour bimodality, with colours of $g - i \sim 0.9$ and 1.2 down to magnitudes of $i \sim 24$; fainter than that a broad colour distribution is seen. The contribution of contaminating background objects rises steeply at magnitudes fainter than $i = 23.6$. This magnitude also corresponds to reasonable errors of ± 0.05 in i magnitude and ± 0.08 in colour. Thus we now only consider objects brighter than $i = 23.6$. Our bright magnitude limit is chosen to be $i = 20$ ($M_I = -11.12$) as the few sources brighter than this are likely to be foreground stars or compact dwarf galaxies. We note in passing that the number of *potential* ultracompact dwarfs (UCDs; Drinkwater et al. 2003) with $-12.12 < M_I < -11.12$ and $g - i \sim 1$ is about half a dozen. All of these could be foreground stars (see Ratnatunga & Bahcall 1985) suggesting that NGC 4649 does not contain a large population of UCDs. A generous colour range of 0.5 to 1.5 has also been applied for GC selection. Such a selection would include all Milky Way GCs after a reddening correction. These magnitude and colour constraints are shown in

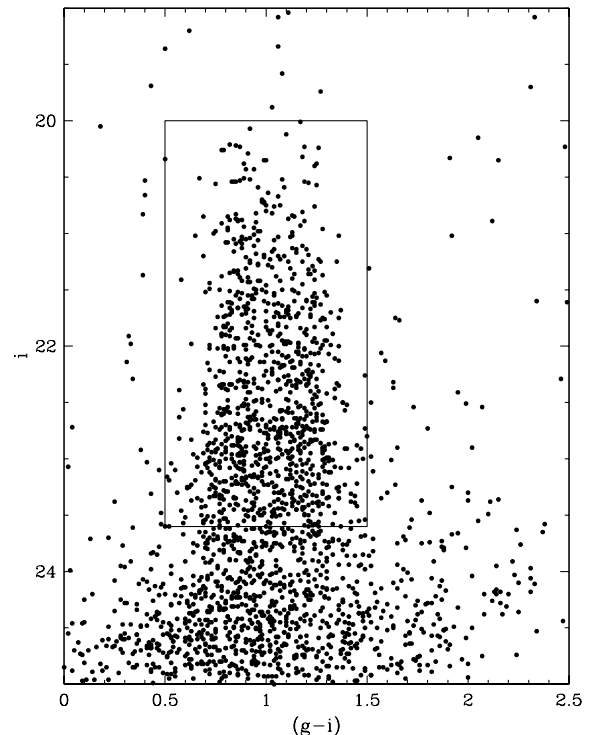


Figure 9. Colour–magnitude diagram for candidate GCs. There is some evidence of a bimodal colour distribution at bright magnitudes. The box shows our selected colour and magnitude region for subsequent analysis.

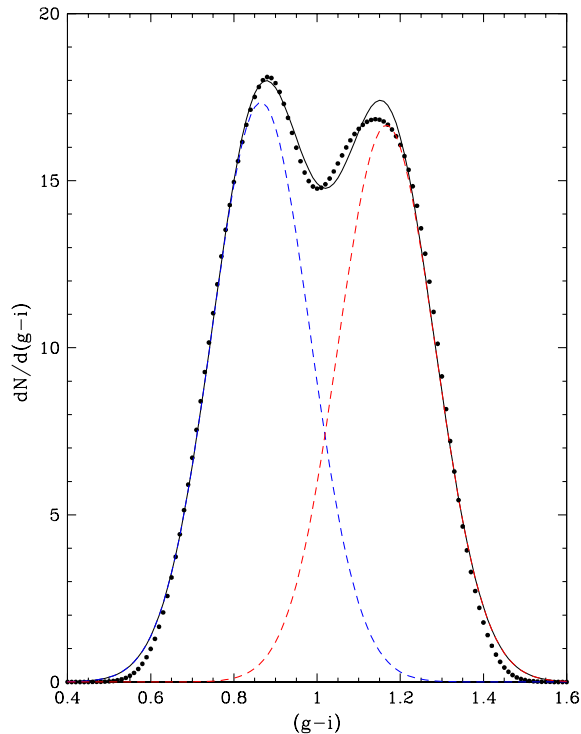


Figure 10. Colour distribution of the magnitude-limited sample of candidate GCs. The data, smoothed by 0.05 mag, are shown by small filled circles. The dashed lines represent a Gaussian fit to the blue and red subpopulations, with the solid line showing the combined fit. Peaks are found at $g - i = 0.87$ and 1.17 .

Fig. 9 and used for the subsequent analysis. A total of 995 objects meet these selection criteria.

In Fig. 10 we show the colour distribution, smoothed on 0.05-mag scales, for the candidate GCs from the CMD selected region. Two Gaussians have been fitted (using `GAUSS` in `IRAF`) to the distribution allowing their amplitudes, central position and FWHM to vary. We find that the distribution is well fitted by two Gaussians. The blue subpopulation has a peak color of $g - i = 0.865 \pm 0.005$, and the red subpopulation has $g - i = 1.167 \pm 0.004$ (an extinction correction would make these colours 0.02–0.05 bluer).

In Fig. 11 we show colour distributions, smoothed on 0.05-mag scales, of candidate GCs over three radial bins (45–90, 90–150 and 150–240 arcsec), all of which have a completeness of ~ 90 per cent or better. These figures show how the inner regions are dominated by red (metal-rich) GCs, the outer regions by blue (metal-poor) GCs and the intermediate regions have similar numbers of the two GC subpopulations.

In Fig. 12 we show the radial gradient of the GC subpopulations compared to the overall GC system and the underlying galaxy starlight. For the galaxy profile two different sky subtraction algorithms have been used; for one the sky level has been subtracted using the counts in the outer regions of our field-of-view, and for the second these counts have been reduced by ~ 75 per cent (under the assumption that the outer regions still contains galaxy light). Both the red and blue GC subpopulations are statistically consistent with no radial colour trend (having non-zero slopes of 2σ and 1.5σ , respectively). However, the overall GC population has a radial colour trend of 6σ significance, becoming bluer with radius. This is therefore the effect of the changing relative mix of GCs with radius, i.e. the ratio of red-to-blue GCs decreases with radius.

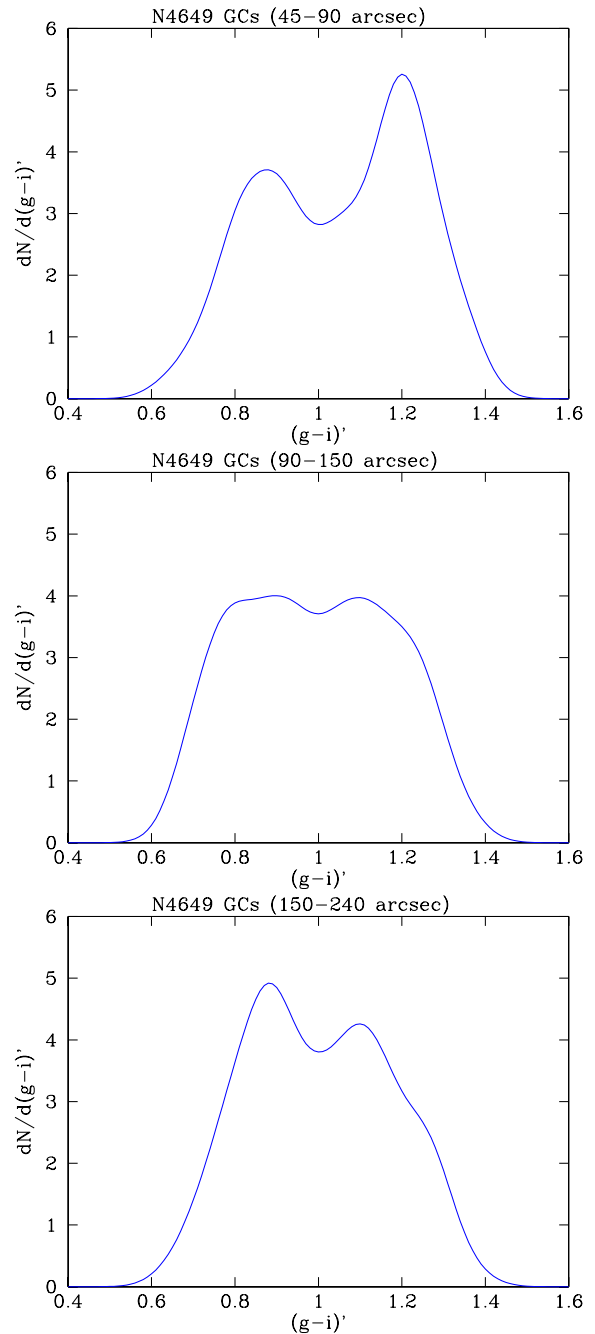


Figure 11. Colour distributions of the candidate GCs. The figure shows three radial bins, smoothed by 0.05 mag. Top: 45–90 arcsec; middle: 90–150 arcsec; bottom: 150–240 arcsec. The red GCs dominate the inner regions.

Similar trends been found over the radial range observed here for NGC 4472 (Geisler, Lee & Kim 1996; Rhode & Zepf 2001) and NGC 1399 (Forbes et al. 1998; Dirsch et al. 2003). The galaxy light has a similar colour to the mean colour of the red GCs for common radii (see also Forbes & Forte 2001).

5.2 Globular cluster surface density

In Fig. 13 we show the surface density of the two GC subpopulations versus galactocentric radius. A correction has been made for the

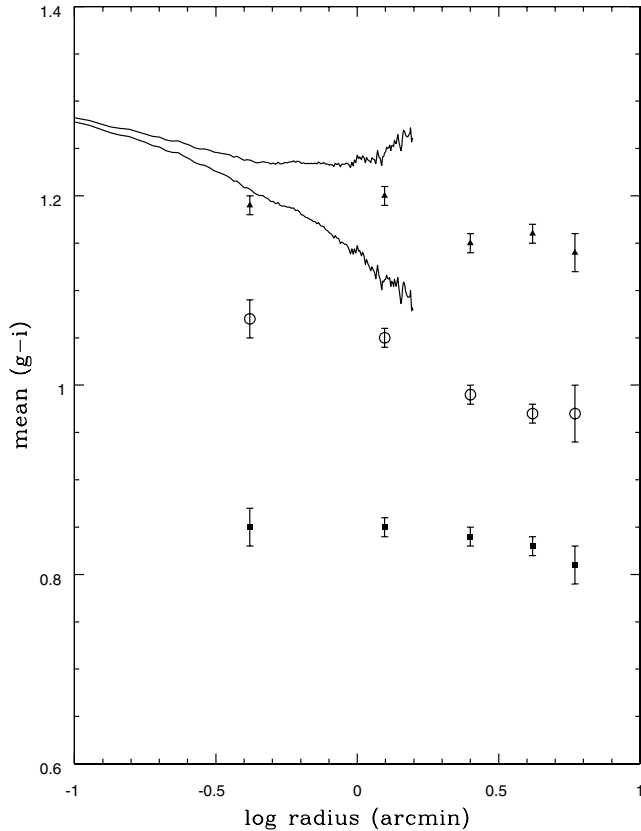


Figure 12. Globular cluster mean colour gradients. The red (triangles) and blue (squares) GC subpopulations are shown along with the total GC population (circles). Poisson error bars are given. The solid lines show the $g - i$ colour profile of the underlying galaxy starlight for two different sky subtractions. Both the red and blue GC subpopulations are consistent with no radial trend, whereas the overall GC population becomes bluer with radius. The galaxy light is more similar in colour to the red GCs than the blue subpopulation.

missing area in each radial annulus. The error bars correspond to Poisson statistics.

As expected from Fig. 11, we find the red GCs are more concentrated towards the galaxy centre than the blue GCs. In other words, the red GCs have a steeper surface density profile. A simple power-law fit to the surface density profiles gives a slope of -1.73 ± 0.06 for the reds and -1.04 ± 0.09 for the blues. We note that Harris et al. (1991) measured a slope of -1.08 ± 0.10 for the overall GC system out to radii of 140 arcsec (for comparison our overall slope measured out to 230 arcsec is -1.3 ± 0.05).

Fig. 13 also shows the galaxy i -band surface brightness profile, after converting into log units and applying an arbitrary vertical normalization. The slope of the galaxy profile changes from -1.45 ± 0.02 in the inner regions (5 to 30 arcsec) to -1.75 ± 0.02 in the outer regions (30 to 230 arcsec). Thus for the region of overlap with the GC system, the galaxy starlight has the same slope, within the errors, to that of the red GC subpopulation.

5.3 GC specific frequency

Given our somewhat uncertain photometric calibration, we will not attempt a detailed analysis of the GC luminosity function for NGC 4649. However, we can still usefully estimate the total number of GCs in the NGC 4649 system, and hence the GC specific frequency.

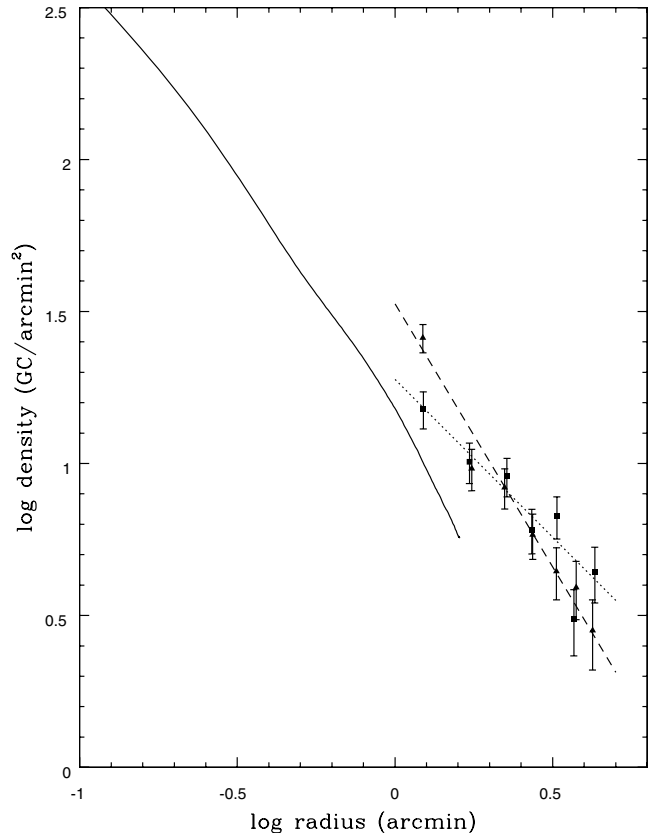


Figure 13. Globular cluster surface density profiles. The red (triangles) and blue (squares) GC subpopulations are shown separately. Poisson error bars are given. The dashed line shows the best fit to the red GCs with power slope of -1.73 , and the dotted line the blue fit of -1.04 . The solid line shows the galaxy starlight profile, which has a slope consistent with the red GCs.

We have corrected the counts, in 0.25-mag bins, for our incompleteness as a function of galactocentric radius and magnitude. As mentioned in Section 3.4, for $i < 23.6$ we have essentially detected all GCs over the field-of-view of our observations. We need to make two corrections in order to estimate the total number of GCs in the system. The first concerns the missing areal coverage, i.e. beyond 230 arcsec, and the second concerns GCs fainter than the limiting magnitude of $i = 23.6$.

By integrating the surface density profile from 60 to 230 arcsec we estimate 1007 GCs. Interior to 60 arcsec we assume a constant GC number density as adopted by Harris et al. (1991). This gives another 219 GCs. Extrapolating the surface density profile out to 10 arcmin or 48.6 kpc (such large radial extents have been observed for giant ellipticals in clusters) gives an additional 1421 GCs.

Thus we estimate the total number of GCs spatially to be 2647 but this is only to magnitudes of $i = 23.6$. In Fig. 14 we show the completeness and background corrected GC luminosity function in 0.25-mag bins. The corrected counts show a steady Gaussian-like rise profile. We have fit the data using NGAUSS in IRAF and find a Gaussian profile of width $\sigma = 1.30 \pm 0.1$ mag (Harris et al. 1991 found $\sigma = 1.29$ and Larsen et al. 2001 measured $\sigma = 1.28$) and a peak or turnover magnitude of $i = 23.17 \pm 0.15$. The resulting Gaussian profile is shown in Fig. 14 to be a reasonable fit to the data. This profile has about 62 per cent of GCs brighter than $i = 23.6$ (the limit used in the density analysis) and 38 per cent fainter.

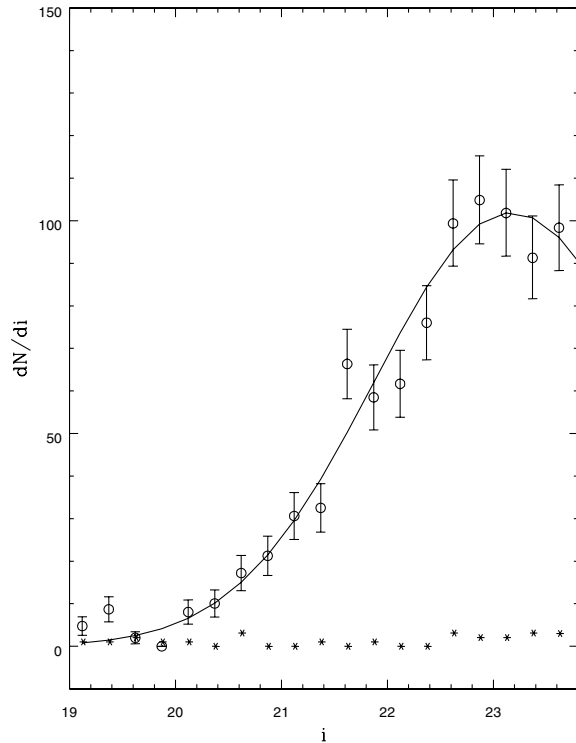


Figure 14. Globular cluster luminosity function. The data, in 0.25-mag bins, are shown by open circles with Poisson error bars. The data have been corrected for incompleteness and background contamination (the background level is shown by stars). The solid line shows a Gaussian fit to the data for magnitudes $i < 23.6$. The fit has a peak or turnover magnitude at $i = 23.17$, and a dispersion $\sigma = 1.30$.

We estimate the total number of GCs in the NGC 4649 system, integrated over all magnitudes and area, to be 3653. Various random errors are present in this estimate, but the largest uncertainty is probably associated with the extrapolation of the surface density to large radii not covered by our images. For example, if we had chosen 8 or 12 arcmin, instead of 10 arcmin, for the radial extent our estimate would change by ± 25 per cent. In addition, the true surface density profile might not be a single power-law at all radii (Rhode & Zepf 2004; Dirsch et al. 2003). A remaining systematic error is that of the photometric calibration. These caveats aside, our final estimate of the total GC population is 3700 ± 900 which is less than the 5100 ± 1100 given in the compilation of Ashman & Zepf (1998). This value is based on observations by Harris et al. (1991). We derive a steeper density profile than Harris et al., and hence a smaller GC population.

For an absolute magnitude of $M_V = -22.38$, we estimate a global specific frequency of $S_N = 4.1 \pm 1.0$. This is fairly typical of cluster ellipticals, and less than the 6.7 ± 1.4 in Ashman & Zepf (1998). We also note that, because the ratio of red-to-blue GCs decreases with radius (see Section 5.1), the *local* S_N value for red GCs will decrease relative to the blue S_N with galactocentric radius.

6 DISCUSSION AND CONCLUSIONS

Our two-filter imaging of the NGC 4649 GC system has returned a number of results. However, before turning to GCs, we confirm the findings of White et al. (2000), that any possible foreground extinction due to the disc of NGC 4647 is limited to be less than

~ 0.1 mag. We also argue that the number of UCDs associated with NGC 4649 is small, i.e. less than half a dozen.

With the caveat that the GMOS photometric calibration is not final, we detect GC colour bimodality with subpopulations at $g - i = 0.865 \pm 0.005$ and 1.167 ± 0.004 (an extinction correction would make these colours 0.02–0.05 bluer).

As is commonly seen in other galaxies, the red GCs are concentrated towards the centre of the galaxy. They have a steep number density profile of slope -1.73 ± 0.06 compared to the shallower slope of -1.04 ± 0.09 for the blues. The varying ratio of red-to-blue GCs with radius can largely explain the overall GC system colour gradient.

For common radii, the underlying galaxy starlight has a similar density profile to the red GCs and colour to the mean colour of the red GCs. This suggests similar metallicities and/or ages (formation epoch) for the red GCs and the galaxy field stars. A luminosity-weighted spectral age based on Lick indices (Terlevich & Forbes 2002) suggests that the galaxy stars are old. The fact that the peak of the red GC luminosity function is fainter than that for the blue GCs (Larsen et al. 2001) is consistent with an old age for the GCs, as at a given age metal-rich GCs are expected to be fainter than metal-poor GCs due to line blanketing effects. Our forthcoming GMOS spectra will have sufficient S/N to derive Lick style ages for the brighter GCs (Bridges et al., in preparation).

We estimate a total GC population of 3700 ± 900 , which corresponds to a specific frequency $S_N = 4.1 \pm 1.0$. This is lower than the current value quoted in the literature.

ACKNOWLEDGMENTS

We thank the Gemini support staff for their help. We thank R. Musgrave for help preparing some of the figures, and M. Pierce for his comments on the text. We also thank the referee, S. Larsen, for suggested improvements to the paper. These data were based on observations obtained at the Gemini Observatory, which is operated by the Association of Universities for Research in Astronomy, Inc., under a cooperative agreement with the NSF on behalf of the Gemini partnership: the National Science Foundation (United States), the Particle Physics and Astronomy Research Council (United Kingdom), the National Research Council (Canada), CONICYT (Chile), the Australian Research Council (Australia), CNPq (Brazil), and CONICET (Argentina). The Gemini program ID is 20020410-GN-2002A-Q-21/Q-13. This work was supported in part by a research grant provided to DAH by the Natural Science and Engineering Research Council of Canada.

REFERENCES

- Ashman K. M., Zepf S. E., 1992, *ApJ*, 384, 50
- Ashman K. M., Zepf S. E., 1998, *Globular Cluster Systems*. Cambridge University Press, Cambridge
- Beasley M. A., Baugh C. M., Forbes D. A., Sharples R. M., Frenk C. S., 2002, *MNRAS*, 333, 383
- Bertin E., Arnouts S., 1996, *A&AS*, 117, 393
- Bridges T. J. et al., 2003, in Bridges T., Forbes D., eds, 25th IAU General Assembly, JD6, Extragalactic Globular Clusters and their Host Galaxies. Astron. Soc. Pac., San Francisco, in press (astro-ph/0310324)
- Bridges T. J., Ashman K. M., Zepf S. E., Carter D., Hanes D. A., Sharples R. M., Kavelaars J. J., 1997, *MNRAS*, 284, 376
- Brocato E., Castellani V., Poli F., Raimondo G., 2000, *A&AS*, 146, 91
- Burstein D., Heiles C., 1982, *AJ*, 87, 1165
- Cote P., Marzke R. O., West M. J., 1998, *ApJ*, 501, 554

Couture J., Harris W. E., Allwright J. W. B., 1991, *ApJ*, 372, 97
 Dirsch B., Richtler T., Geisler D., Forte J., Bassino L., Gieren W., 2003, *AJ*, 124, 1908
 Drinkwater M., Gregg M. D., Hilker M., Bekki K., Couch W. J., Ferguson H. C., Jones J. B., Phillipps S., 2003, *Nat*, 423, 519
 Forbes D. A., Brodie J. P., Grillmair C. J., 1997, *AJ*, 113, 1652
 Forbes D. A., Grillmair C. J., Williger G. M., Elson R. A. W., Brodie J. P., 1998, *MNRAS*, 293, 325
 Forbes D. A., Forte J. C., 2001, *MNRAS*, 322, 257
 Gebhardt K., Kissler-Patig M., 1999, *AJ*, 118, 1526
 Geisler D., Lee M. G., Kim E., 1996, *AJ*, 111, 1529
 Harris W. E., Allwright J. W. B., Pritchett C. J., van den Bergh S., 1991, *ApJS*, 76, 115
 Harris W. E., 2001, in Labhardt L., Binggel B., eds, *Star Clusters. SAAS-Fee Advanced Course 28*, p. 223
 Kundu A., Whitmore B. C., 2001, *AJ*, 122, 1251
 Larsen S. S., Brodie J. P., Huchra J. P., Forbes D. A., Grillmair C. J., 2001, *AJ*, 121, 2974
 O'Sullivan E., Forbes D., Ponman T., 2001, *MNRAS*, 328, 461
 Ratnatunga K., Bahcall J., 1985, *ApJS*, 59, 63
 Rhode K., Zepf S., 2001, *AJ*, 121, 210
 Rhode K., Zepf S., 2004, *AJ*, 127, 302
 Sarazin C., Kundu A., Irwin J., Sivakoff G., Blanton E., Randall S., 2003, *ApJ*, 595, 743
 Schlegel D. J., Finkbeiner D. P., Davis M., 1998, *ApJ*, 500, 525
 Smith J. et al., 2002, *AJ*, 123, 2121
 Stetson P., 1987, *PASP*, 99, 191
 Terlevich A., Forbes D., 2002, *MNRAS*, 330, 547

Tonry J., Dressler A., Blakeslee J. P., Ajhar E. A., Fletcher A. B., Luppino G. A., Metzger M. R., Moore C. B., 2001, *ApJ*, 546, 681
 White R., Keel W., Conselice C., 2000, *ApJ*, 542, 761

APPENDIX A:

The photometric data for the resolved objects in the field of NGC 4649 are given in Table A1. The magnitudes are not total magnitudes but derived from aperture photometry. The colours however should be largely unaffected.

Table A1. Resolved Objects in the field of NGC 4649.

X (pix)	Y (pix)	R_{GC} (arcsec)	i (mag)	$g - i$ (mag)	i err (mag)	$g - i$ err (mag)
3925	4531	127.7	21.81	-0.30	0.03	0.04
3812	4545	121.1	24.24	-0.35	0.10	0.12
3818	4511	120.3	21.32	-0.02	0.03	0.04
...

Notes: the full table is available in the on-line version at <http://www.blackwellpublishing.com/products/journals/suppmat/MNR/MNR8333/MNR8333sm.htm>

This paper has been typeset from a $\text{T}_{\text{E}}\text{X}/\text{L}_{\text{A}}\text{T}_{\text{E}}\text{X}$ file prepared by the author.